

QCOMMUTE: a tool for symbolic computation of nested commutators in quantum many-body spin-1/2 systems

Oleg Lychkovskiy^{1,2}, Viacheslav Khrushchev³ and Ilya Shirokov^{1,4*}

¹ Skolkovo Institute of Science and Technology,
Bolshoy Boulevard 30, bld. 1, Moscow 121205, Russia

² Department of Mathematical Methods for Quantum Technologies,
Steklov Mathematical Institute of Russian Academy of Sciences,
8 Gubkina St., Moscow 119991, Russia

³ HSE University, 20 Myasnitskaya Ulitsa, Moscow, 101000, Russia

⁴ Moscow State University, Faculty of Physics, Moscow, 1199991 Russia

* shirokovie@my.msu.ru

Abstract

We present QCOMMUTE [1], a software tool implemented in C++ for symbolic computation of nested commutators between a Hamiltonian and local observables in quantum many-body spin-1/2 systems on one-, two-, and three-dimensional hypercubic lattices. The computation is performed algebraically directly in the thermodynamic limit, and the Hamiltonian parameters are kept symbolic. Importantly, this way the entire parameter space is covered in a single run. The implementation supports extensive parallelization to achieve high computational performance. QCOMMUTE enables the investigation of quantum dynamics in strongly correlated regimes that are inaccessible to perturbative approaches, either through direct Taylor expansion in time or via advanced techniques such as the recursion method.

Copyright attribution to authors.

This work is a submission to SciPost Physics Codebases.

License information to appear upon publication.

Publication information to appear upon publication.

Received Date

Accepted Date

Published Date

Contents

1	Introduction	2
2	Physical background	3
2.1	Quantum evolution in the Heisenberg picture	3
2.2	Pauli strings	4
2.3	Translation invariance	5
3	Algorithm and implementation	7
3.1	Algorithm	7
3.2	Implementation	8
3.3	Installing and running QCOMMUTE	9
3.4	Crosschecks	12
3.5	Performance	12

4	An application: short-time dynamics of quantum Ising model	14
5	Summary and outlook	15
	References	16

1 Introduction

Quantitatively describing quantum many-body dynamics in nonperturbative regimes is, in general, a difficult task. While in one dimension a decisive progress has been achieved using matrix product state (MPS) techniques [2–4], in two and especially three dimensions the problem remains largely open. A variety of approaches have been developed to tackle this problem, including variational and Monte-Carlo methods based on tensor network [5–12] or neural network [12–17] representations of quantum many-body states, as well as hybrid quantum-classical approaches [18]. These methods are typically formulated in the Schrödinger picture of quantum mechanics.

More recently, methods operating in the Heisenberg picture have attracted increasing attention [19–26] and, in some cases, have demonstrated performance comparable to or exceeding that of more traditional Schrödinger-picture approaches [23, 26–31]. Most importantly, these include the recursion method [19, 23, 32, 33] and the sparse Pauli dynamics method [27, 28]. The core computational primitive underlying all such Heisenberg methods is the evaluation of commutators $[H, A]$ between a many-body Hamiltonian and an observable. The overall efficiency of Heisenberg methods hinges on the efficiency of the implementation of this core primitive.

Recently, the Julia package PAULISTRINGS.JL has been released, providing an implementation of this primitive for spin-1/2 systems and building upon it to implement the recursion method [34, 35]. Another recent package with a related functionality, PAULIPROPAGATION.JL [36], places emphasis on the simulation of quantum circuits and sparse Pauli dynamics, with the additional capability to incorporate dissipation. A Python implementation used in the original sparse Pauli dynamics works [27, 28] is also publicly available [37]. Other groups working in the field have developed their own software [19, 38–43] that has not been publicly released.

In this work, we present QCOMMUTE [1], a tool for computing commutators in quantum translation-invariant spin-1/2 systems on hypercubic lattices. Written in C++, QCOMMUTE is designed for high computational efficiency, supports extensive parallelization, operates symbolically (retaining Hamiltonian parameters in analytic form), and works directly in the thermodynamic limit. We have recently employed QCOMMUTE to implement the recursion method for describing quench dynamics in one-, two-, and three-dimensional many-body systems [30]. Here, we describe the inner workings of the code and provide guidance for users. As an illustration, we present results on quantum many-body dynamics derived from the Taylor expansion of Heisenberg operators – a conceptually simple approach that nevertheless yields remarkably accurate results and, in some cases, provides rigorous and extremely tight upper and lower bounds for dynamical quantities at early evolution times.

The rest of the paper is organized as follows. In the next section, we provide the necessary physical background and introduce the required notation, including the basics of quantum dynamics in the Heisenberg picture, as well as properties of Pauli strings and translation-invariant operators constructed from them. In Section 3, we present the algorithm underlying QCOM-

MUTE and its C++ implementation, outline installation and usage, and discuss performance. In Section 4, we apply QCOMMUTE to benchmark the short-time dynamics of exemplary spin systems. In the final section, we summarize main features and capabilities of the package and highlight promising directions for future developments.

2 Physical background

2.1 Quantum evolution in the Heisenberg picture

A Heisenberg operator A_t of a quantum observable is obtained from the Schrödinger operator A of the same observable according to

$$A_t = e^{itH} A e^{-itH} = e^{it\mathcal{L}} A. \quad (1)$$

Here H is the Hamiltonian and

$$\mathcal{L} \equiv [H, \bullet] \quad (2)$$

is a *superoperator* (i.e. a linear map in the space of operators) referred to as Liouvillian. Both A and A_t , as well as H , are self-adjoint operators.

In the many-body setting, A_t can not be, in general, found explicitly (except noninteracting and certain interacting integrable models [44–49]). Rather, it is to be approximated. As a rule, building blocks of such approximations are nested commutators

$$\mathcal{L}^n A = \underbrace{[H, [H, \dots, [H, A] \dots]]}_{n \text{ times}}, \quad (3)$$

where n is referred to as *nesting order*. The most straightforward approximation to A_t is obtained by truncating the Taylor expansion

$$A_t = \sum_{n=0}^{\infty} \frac{(it)^n}{n!} \mathcal{L}^n A \quad (4)$$

at some $n = n_{\max}$, which is the maximal nesting order we are able to explicitly compute. More generally, one has a vast freedom to organize nested commutators in various linear combinations to improve the convergence, according to the formula

$$A_t = \sum_{n=0}^{\infty} \varphi_n(t) P_n(\mathcal{L}) A, \quad (5)$$

where $\{P_n(z)\}$ is a sequence of orthogonal polynomials and $\{\varphi_n(t)\}$ is a related sequence of functions [50]. In particular, the recursion method can be viewed as a specific implementation of the expansion (5), based on a sequence of orthogonal polynomials tailored to the given H and A [50]. An alternative Heisenberg-picture approach, sparse Pauli dynamics [26–28], is based on the trotterization of the unitary evolution in Eq. (1) and, at its computational core, likewise relies on the evaluation of commutators.

If one is able to compute A_t , two physical objects become immediately accessible. The first is the time-dependent post-quench expectation value, i.e. the evolving expectation value of the observable after initialization in a state ρ_0 (assuming ρ_0 is explicitly known):

$$\langle A \rangle_t = \text{tr} \rho_0 A_t. \quad (6)$$

The second is the infinite-temperature autocorrelation function of the observable,

$$C(t) = \text{tr} A A_t / \text{tr} A^2. \quad (7)$$

It is worth noting that finite-temperature correlation functions can also be accessed, albeit using a considerably more sophisticated technique [51].

In the present paper, we introduce a software tool QCOMMUTE that efficiently computes nested commutators (3) for spin-1/2 systems on hypercubic lattices. As an illustration of its performance, we compute approximate post-quench expectation values $\langle A \rangle_t$ and autocorrelation functions $C(t)$ for representative models. To this end, we employ the straightforward Taylor expansion (4), which requires essentially no additional theoretical machinery, in contrast to more sophisticated approaches such as the recursion method. Specifically, we compute

$$\langle A_t \rangle \simeq \sum_{n=0}^{n_{\max}} \frac{q_n}{n!} t^n, \quad (8)$$

$$q_n \equiv \text{tr}(\rho_0 (i\mathcal{L})^n A) \quad (9)$$

and

$$C(t) \simeq \sum_{n=0}^{n_{\max}} (-1)^n \frac{t^{2n}}{(2n)!} \mu_{2n}, \quad (10)$$

$$\mu_{2n} \equiv \text{tr}((i\mathcal{L})^n A)^2 / \text{tr} A^2 \geq 0. \quad (11)$$

We refer to numbers q_n as quench coefficients. Numbers μ_{2n} are commonly known as moments. One obtains eq. (10) from eq. (4) with the help of the identity $\text{tr}(A\mathcal{L}B) = -\text{tr}((\mathcal{L}A)B)$, which implies, in particular, that the odd-order terms in the expansion of $C(t)$ vanish.

A truncated Taylor expansion of a bounded function of time typically provides an excellent approximation at sufficiently small times but breaks down at larger times. This is precisely the behavior that will be observed below when applying Eqs. (8) and (10).

In fact, in the case of the autocorrelation function, the truncated Taylor expansion (10) yields a stronger result. Since eq. (10) is an alternating series, truncation at even (odd) order gives an upper (lower) bound on the value of the function, provided that, starting from some $n < n_{\max}$, the absolute values of the series terms decrease monotonically.¹ This assumption is, in fact, well justified: it is consistent with the universal operator growth hypothesis [19] and with all case studies considered here and elsewhere [23, 29–31]. Under this assumption, we get inequalities

$$\sum_{n=0}^{n_{\max}^{\text{odd}}} (-1)^n \frac{t^{2n}}{(2n)!} \mu_{2n} \leq C(t) \leq \sum_{n=0}^{n_{\max}^{\text{even}}} (-1)^n \frac{t^{2n}}{(2n)!} \mu_{2n}, \quad (12)$$

where n_{\max}^{even} and n_{\max}^{odd} are maximal available even and odd nesting orders, respectively. We will see that these inequalities provide very tight bounds useful for benchmarking other, more sophisticated but less controllable methods.

2.2 Pauli strings

We consider systems of spins 1/2 on a hypercubic lattice of dimension $D \in \{1, 2, 3\}$. The lattice is infinite, i.e. no boundaries are assumed. Sites of the lattice are labeled by a D -dimensional integer vector $\mathbf{r} \in \mathbb{Z}^D$. The site with all components of \mathbf{r} equal to 1 is called the *anchor site*. For example, the anchor site for the 3D lattice is labeled by $\mathbf{r} = (1, 1, 1)$.

Operators are expanded in the basis of *Pauli strings*, which are products of Pauli operators on different sites. A Pauli string $P_{\mathbf{v}}$ reads

$$P_{\mathbf{v}} = \prod_{k=1}^w \sigma_{\mathbf{r}_k}^{\alpha_k}. \quad (13)$$

¹We consider only values of t within the radius of convergence of the Taylor expansion, which is finite for two- and three-dimensional systems in the thermodynamic limit [19] and infinite for one-dimensional systems [19, 52].

Here $\sigma_{\mathbf{r}_k}^{\alpha_k}$ with $\alpha_k \in \{x, y, z\}$ is a Pauli matrix on the site \mathbf{r}_k , and the label ν is a shorthand for the multi-index

$$\nu = ((\mathbf{r}_1, \alpha_1), (\mathbf{r}_2, \alpha_2), \dots, (\mathbf{r}_w, \alpha_w)). \quad (14)$$

The set $\text{supp}(P_\nu)$ of site labels alone,

$$\text{supp}(P_\nu) = (\mathbf{r}_1, \mathbf{r}_2, \dots, \mathbf{r}_w), \quad (15)$$

is referred to as the *support* of the Pauli string (13). The identity operator is also regarded to be a Pauli string.

The site labels \mathbf{r}_k in eqs. (14),(15) are ordered lexicographically. We refer to the site \mathbf{r}_1 in eqs. (14),(15) as the first site of the Pauli string. A Pauli string \check{P}_ν is *anchored* if its first site is the anchor site (e.g. $\mathbf{r}_1 = (1, 1, 1)$ in the 3D case); the check mark on top of \check{P}_ν distinguishes anchored Pauli strings \check{P}_ν from general Pauli strings P_ν .

Two important properties of a Pauli string are its *weight* and *size*. The weight $w(P_\nu)$ is the number of Pauli matrices in the Pauli string P_ν . The size $s(P_\nu)$ is the length of the edge of the smallest hypercube that contains the support $\text{supp}(P_\nu)$ of the Pauli string.

A product of two Pauli strings is also a Pauli string, perhaps multiplied by (-1) or $(\pm i)$. This product is computed site-wise using identities

$$\sigma_{\mathbf{r}}^\alpha \sigma_{\mathbf{r}}^\beta = \delta_{\alpha\beta} \mathbb{1}_{\mathbf{r}} + i \sum_{\gamma} \varepsilon_{\alpha\beta\gamma} \sigma_{\mathbf{r}}^\gamma, \quad \alpha, \beta, \gamma \in x, y, z. \quad (16)$$

The commutator $[P_\nu, P_{\nu'}]$ of two Pauli strings is either zero or again a Pauli string, up to a multiplicative numerical coefficient. If the supports of the two Pauli strings do not overlap, their commutator vanishes. The weight and the size of the commutator is limited by the respective weights and sizes of the Pauli strings as follows:

$$w([P_\nu, P_{\nu'}]) \leq w(P_\nu) + w(P_{\nu'}) - 1 \quad (17)$$

$$s([P_\nu, P_{\nu'}]) \leq s(P_\nu) + s(P_{\nu'}) - 1 \quad (18)$$

2.3 Translation invariance

We address only translation-invariant Hamiltonians and observables. As an example, consider the transverse-field Ising Hamiltonian,

$$H = \sum_{\langle \mathbf{r}\mathbf{r}' \rangle} \sigma_{\mathbf{r}}^x \sigma_{\mathbf{r}'}^x + h_z \sum_{\mathbf{r}} \sigma_{\mathbf{r}}^z, \quad (19)$$

and the operator of the per-site magnetization along the z direction,

$$A = N^{-1} \sum_{\mathbf{r}} \sigma_{\mathbf{r}}^z. \quad (20)$$

The sum in eq. (20) and the second sum in eq.(19) run over all lattice sites, while the first sum in eq.(19) runs over the pairs $\langle \mathbf{r}\mathbf{r}' \rangle$ of neighboring sites (i.e. over all edges) of the hypercubic lattice. The normalization factor N^{-1} (N being the total number of lattice sites) ensures that the observable is intensive (does not scale in the thermodynamic limit). This factor is purely formal: it cancels in all end results, see eqs. (28) and (30) below.

To represent translation-invariant operators compactly, we introduce a linear superoperator \mathcal{T} that distributes a local operator over the hypercubic lattice. Specifically, \mathcal{T} maps a Pauli string P_ν to the sum of all strings obtained from P_ν by all possible translations in all D spatial directions. For example, for $D = 3$, the Ising Hamiltonian (19) and the magnetization (20) can be written as

$$H = \mathcal{T} \left(\sigma_{(1,1,1)}^x \sigma_{(2,1,1)}^x + \sigma_{(1,1,1)}^x \sigma_{(1,2,1)}^x + \sigma_{(1,1,1)}^x \sigma_{(1,1,2)}^x + h_z \sigma_{(1,1,1)}^z \right), \quad (21)$$

and

$$A = N^{-1} \mathcal{T} \sigma_{(1,1,1)}^z, \quad (22)$$

respectively. Here site labels are shown as explicit D -dimensional vectors.

We say that a translation-invariant operator A is in the *canonical form* if it can be represented as

$$A = \mathcal{T} a \quad (23)$$

where the *density* a is a linear combination of anchored Pauli strings,

$$a = \mathcal{T} \sum_{\nu} c_{\nu} \check{P}_{\nu}. \quad (24)$$

We always assume that this sum contains a finite number of terms. Operators H and A in Eqs. (21) and (22), respectively, are written in the canonical form.

The key property of \mathcal{T} is that it commutes with \mathcal{L} whenever the corresponding Hamiltonian is translation-invariant. This allows one to simplify the computation of $\mathcal{L}A$ when A is also translation-invariant:

$$\mathcal{L}A = N^{-1} \mathcal{L} \mathcal{T} a = N^{-1} \mathcal{T} \mathcal{L} a. \quad (25)$$

This way, we first compute the commutator between H and the density a of the observable A (remind that a is a finite sum of Pauli strings), and then distribute the result over the whole lattice. Note that at the latter step every two Pauli strings that can be obtained from one another by some translation collapse to a single term, e.g.

$$\mathcal{T}(\sigma_1^y \sigma_2^x + \sigma_2^y \sigma_3^x) = \mathcal{T}(\sigma_1^y \sigma_2^x) + \mathcal{T}(\sigma_2^y \sigma_3^x) = \mathcal{T}(\sigma_1^y \sigma_2^x) + \mathcal{T}(\sigma_1^y \sigma_2^x) = \mathcal{T}(2\sigma_1^y \sigma_2^x), \quad (26)$$

where $D = 1$ is assumed. In the software implementation, this consequence of translation invariance leads to considerable memory savings.

Assume one has computed the n 'th nested commutator and represented it in the canonical form,

$$\mathcal{L}^n A = N^{-1} \mathcal{T} \sum_{\nu} c_{\nu}^{(n)} \check{P}_{\nu}, \quad (27)$$

where the $c_{\nu}^{(n)}$ are numerical coefficients that are real (imaginary) for even (odd) n . Then one immediately obtains the $(2n)$ 'th moment (11):

$$\mu_{2n} = \sum_{\nu} |c_{\nu}^{(n)}|^2 / \sum_{\nu} |c_{\nu}^{(0)}|^2. \quad (28)$$

Here $c_{\nu}^{(0)}$ are expansion coefficients of the density a of the observable A : $a = \sum_{\nu} c_{\nu}^{(0)} \check{P}_{\nu}$.

To obtain quench coefficients (9), an initial state should be specified. We focus on translation-invariant product states

$$\rho_0 = \bigotimes_{\mathbf{r}} \frac{1}{2} (\mathbb{1}_{\mathbf{r}} + \mathbf{p} \boldsymbol{\sigma}_{\mathbf{r}}), \quad (29)$$

where $\mathbf{p} \boldsymbol{\sigma}_{\mathbf{r}} \equiv p_x \sigma_{\mathbf{r}}^x + p_y \sigma_{\mathbf{r}}^y + p_z \sigma_{\mathbf{r}}^z$ and \mathbf{p} is a real three-dimensional *polarization vector* satisfying $|\mathbf{p}| \leq 1$.

For this initial state the n 'th quench coefficient (9) reads

$$q_n = \sum_{\nu} c_{\nu}^{(n)} \Upsilon(\check{P}_{\nu}). \quad (30)$$

Here $\Upsilon(P_{\nu})$ is a real number obtained from the Pauli string P_{ν} by substituting each Pauli matrix by a corresponding component of the polarization vector, $\sigma_{\mathbf{r}}^{\alpha} \rightarrow p_{\alpha}$, e.g.

$$\Upsilon(\sigma_0^y \sigma_5^x \sigma_6^y \sigma_8^z) = p_x p_y^2 p_z. \quad (31)$$

The notions of weight and size of a Pauli string can be extended to an arbitrary operator. To this end, one expands the operator in the basis of Pauli strings and defines its weight (size) as the maximum of the weights (sizes) of the Pauli strings appearing in the expansion with nonzero coefficients. For example, $w(H) = s(H) = 2$ for the Ising Hamiltonian (19).

It is easy to see that inequalities (17),(18) hold for arbitrary operators. In particular, inequality (18) implies that the action of the Liouvillian increases the size of an operator by at most $(s(H) - 1)$. One consequence is that the computation of $\mathcal{L}^n A$ yields essentially identical results for a system on an infinite lattice and for a finite system with periodic boundary conditions, provided that its linear size exceeds $s(A) + n(s(H) - 1)$. This observation should be kept in mind when comparing results for infinite and finite systems.

3 Algorithm and implementation

3.1 Algorithm

The algorithm iteratively computes the sequence of nested commutators $A^{(n)}$ defined by

$$A^{(0)} = A \quad (\text{initial observable}), \quad (32)$$

$$A^{(n+1)} = \mathcal{L}A^{(n)} \equiv [H, A^{(n)}]. \quad (33)$$

As long as the observable A and the Hamiltonian H are translation-invariant, they are determined by their densities h and a , respectively,²

$$H = \mathcal{T}h, \quad A = N^{-1} \mathcal{T}a, \quad (34)$$

as explained in the previous Section. Nested commutators are also translation-invariant and, therefore, are also determined by their densities. The computation of these densities is simplified by the fact that the Liouvillian and the translation superoperator commute, as described in Eq. (25). Thus, at the highest level, the algorithm is as follows:

Algorithm 1 Computation of nested commutators

- 1: **Input:** density of Hamiltonian h , density of observable a , maximal nesting order n_{\max}
 - 2: **Output:** sequence $\{a^{(n)}\}_{n=0}^{n_{\max}}$ of densities of nested commutators $\mathcal{L}^n A$
 - 3: $a^{(0)} \leftarrow a$
 - 4: **for** $n \leftarrow 1$ to n_{\max} **do**
 - 5: $a^{(n)} \leftarrow \text{Commute}(\mathcal{T}h, a^{(n-1)})$
 - 6: **end for**
 - 7: **return** $\{a^{(n)}\}_{n=0}^{n_{\max}}$
-

The central routine of this algorithm is `Commute`. It performs the following procedure:

²The density h should not be confused with the magnetic field constant h_z entering the Hamiltonian (19).

Algorithm 2 $\text{Commute}(\mathcal{T}h, a)$ routine

```

1: Input: density of Hamiltonian  $h = \sum_{\nu \in \Omega_H} c_\nu^H \check{P}_\nu$ , density of observable  $a = \sum_{\nu \in \Omega_A} c_\nu^A \check{P}_\nu$ 
2: Output: density of the commutator  $[H, A]$ 
3:  $res \leftarrow 0$ 
4: for each  $\nu' \in \Omega_A$  do
5:   for each  $P_\nu$  from  $H = \mathcal{T}h$  such that  $\text{supp}(\check{P}_{\nu'}) \cap \text{supp}(P_\nu) \neq \emptyset$  do
6:      $comm \leftarrow c_\nu^H c_{\nu'}^A [P_\nu, P_{\nu'}]$ 
7:      $res \leftarrow \text{Add}(comm, res)$ 
8:      $res \leftarrow \text{Canonicalize}(res)$ 
9:      $res \leftarrow \text{Simplify}(res)$ 
10:  end for
11: end for
12: return  $res$ 

```

Here, in line 1, sets Ω_H and Ω_A contain labels of anchored Pauli strings that enter h and a , respective. In line 5, one takes every P_ν (not necessarily anchored) that enters H and has a nonzero overlap with an anchored Pauli string $\check{P}_{\nu'}$ from a . In line 6, if P_ν is not anchored, c_ν^H is the coefficient associated to the anchored Pauli string \check{P}_ν , related to P_ν by a translation. In line 8, the `Canonicalize` command brings the operator to the canonical form, replacing each non-anchored Pauli string P_ν by its anchored counterpart \check{P}_ν , related to P_ν by a translation (see eq.(26) for an example). In line 9, the `Simplify` command collects like terms and removes those with zero coefficients (see eq.(26)).

Importantly, all coefficients multiplying Pauli strings in the expansion of $\mathcal{L}^n H$ in the Pauli-string basis are treated symbolically. Specifically, the coefficients of Pauli strings in the Hamiltonian and the observable are restricted to be either integers or symbolic parameters, as in Eqs. (21) and (22). The `Commute` routine is carried out algebraically, so that all coefficients of Pauli strings in $\mathcal{L}^n H$ become polynomials in these parameters with integer coefficients. In what follows, we refer to these polynomials as *coefficient polynomials* for brevity.

3.2 Implementation

The algorithmic framework described in Section 3.1 is implemented in C++17, with a strong focus on high performance and the exactness of symbolic computations. Below we highlight the key architectural features of the `COMMUTE` package:

- **Data structures:** The physical operators are mapped directly to efficient C++ structures. The spatial coordinate of a lattice site, represented mathematically by a D -dimensional integer vector \mathbf{r} , is implemented as a template class `Point<D>`. A local Pauli operator $\hat{\sigma}_{\mathbf{r}}^\alpha$ is represented by the `Sigma` structure, which encapsulates the `Point<D>` coordinate and an integer indicating the Pauli matrix type $\alpha \in \{x, y, z\} \cong \{1, 2, 3\}$. Coefficient polynomials are stored in a dedicated `Poly` class that contains two vectors. The first vector encodes monomial exponents as 8-bit integers, with individual monomials separated by the delimiter value 254 (consequently, the maximum allowed exponent of each variable is 253). The second vector stores the corresponding coefficients as arbitrary-precision integers, as described below.
- **Arbitrary-precision integer arithmetic:** Computing nested commutators generates a combinatorially large number of terms, and the coefficient polynomials (in particular, integer coefficients of these polynomials) grow extremely fast. Standard 64-bit integer types would inevitably overflow for large nesting orders. To prevent this, the code uti-

lizes the GMP library (`gmpxx`) for arbitrary-precision integer arithmetic, ensuring mathematically exact integer coefficients regardless of the nesting order.

- **Disk Swapping and Chunking:** The core challenge of computing nested commutators is the exponential growth of the result with nesting order, which rapidly exhausts available RAM. To circumvent this, COMMUTE does not keep the entire commutator expression in memory. Instead, it dynamically splits the data into manageable chunks and writes intermediate expressions to the disk as binary `.comm` files. These files are stored in dedicated subdirectories, one for each nesting order. This way, the program is able to compute deeply nested commutators even on personal computers.

3.3 Installing and running QCOMMUTE

The COMMUTE package is distributed as open-source software via GitLab [53]. The core computations rely on exact symbolic algebra and arbitrary-precision integer arithmetic. Thus, the only strict external dependency is the GNU Multiple Precision Arithmetic Library (GMP/`gmpxx`). A C++17 compliant compiler, such as GCC or Clang, is required.

Compilation

For UNIX-like environments (Linux, macOS), the recommended approach for compiling the software is utilizing the *Meson* build system:

```
git clone https://gitlab.com/viacheslav_hrushev/commutators
cd commutators
meson setup --buildtype=release build-release
cd build-release
meson compile
```

This sequence configures the project with high optimization flags and produces the executable binary named `main`.

Alternatively, users can compile the program manually directly via GCC. This is particularly useful for Windows users or those utilizing the provided `tasks.json` file in Visual Studio Code. The equivalent manual compilation command reads

```
g++ *.cpp -o main -std=c++17 -O3 -lgmpxx -lgmp
```

Model configuration file

The model, i.e. the Hamiltonian, the observable and the maximal nesting order, is specified via a plain-text configuration file (e.g., `Comm.txt`). The program parses this file to construct symbolic representations of operators. The file consists of three main sections, denoted by `H:`, `O:`, and `n:`.

For example, a configuration file for the Ising Hamiltonian (21) on the cubic lattice, observable (22) and maximal nesting order $n_{\max} = 12$ reads

```
H:
[1]*Sx(1,1,1)*Sx(2,1,1)
[1]*Sx(1,1,1)*Sx(1,2,1)
[1]*Sx(1,1,1)*Sx(1,1,2)
[1,1]*Sz(1,1,1)
O:
[1]*Sz(1,1,1)
```

n:
12

The details of the syntax are as follows.

- **Pauli operators and dimensionality:** $S_x(r_x, r_y, r_z)$, $S_y(r_x, r_y, r_z)$, $S_z(r_x, r_y, r_z)$ stay for σ_r^x , σ_r^y , σ_r^z , respectively, with $\mathbf{r} = (r_x, r_y, r_z)$. The spatial dimension D of the model is implicitly defined by the number of components of \mathbf{r} (e.g. $S_x(1)$ is used in the 1D case, $S_x(1, 1)$ – in the 2D case, and $S_z(1, 1, 1)$ – in the 3D case).
- **Hamiltonian (H:):** The density of the model Hamiltonian is specified as a finite sum of terms, each term being a product of a symbolic coefficient (see below) and an anchored Pauli string.
- **Observable (O:):** The density of the observable is specified analogously to the density of the Hamiltonian. The formal normalization factor N^{-1} is omitted.
- **Nesting order (n:):** A positive integer specifying the maximum nesting order n_{\max} to be computed.

Coefficient polynomial syntax

A key feature of COMMUTE is that coupling constants are treated symbolically as polynomials of abstract system parameters (e.g., h_1, h_2, \dots) with integer coefficients. These coefficient polynomials are encoded in square brackets $[\dots]$. Terms of the polynomial are separated by a semicolon (;). Each term is a comma-separated list where the first number is the integer coefficient, and the subsequent numbers are the powers of the abstract parameters h_i . For example:

- $[1]$ stands for 1.
- $[2, 2]$ stands for $2h_1^2$.
- $[1; 1, 1, 1; 1, 0, 1; 2, 2, 1]$ stands for $1 + h_1h_2 + h_2 + 2h_1^2h_2$.

Execution Pipeline

The execution of the COMMUTE package generally follows a two-step pipeline: computing nested commutators up to the given nesting order n_{\max} and subsequently post-processing them to extract moments (11) or quench coefficients (9).

Step 1: Computing nested commutators

To compute nested commutators from a given input file, the executable is invoked with a path to the output file. By default, the program outputs the results into a `./tmp` directory, but a custom output directory can be specified using the `-res-dir` flag:

```
./main Comm.txt --res-dir ./results_dir
```

To manage memory efficiently, the program does not keep all commutators in RAM. Instead, it creates a subdirectory for each nesting order (e.g., 0, 1, ..., n) containing binary `.comm` files with the computed Pauli strings.

Step 2: Post-processing

Once the commutators are generated, the user can invoke specific sub-commands pointing to the generated directory to extract moments (28) or quench coefficients (30).

To compute moments (28), the momentum sub-command is invoked:

```
./main momentum ./results_dir > momentums.txt
```

The resulting moments are (in general, multivariate) polynomials of the model parameters with integer coefficients. The output file is produced in WOLFRAM MATHEMATICA[®]-readable form, with the Hamiltonian parameters denoted by h_0, h_1, \dots . For example, for the 1D mixed-field Ising model, whose Hamiltonian (35) contain two parameters (see below), the magnetization (20) as the observable and the nesting order $n_{\max} = 3$, the output file reads

```
moments = {
8 + 4 h0^2,
128 + 128 h1^2 + 192 h0^2 + 16 h0^2 h1^2 + 16 h0^4,
2048 + 6144 h1^2 + 2048 h1^4 + 7680 h0^2 + 5888 h0^2 h1^2 + 64 h0^2
h1^4 + 1920 h0^4 + 128 h0^4 h1^2 + 64 h0^6
};
```

To compute quench coefficients (30), the quench sub-command is used:

```
./main quench ./results_dir > quenches.txt
```

The resulting quench coefficients are multivariate polynomials of the model parameters and components of the polarization vector \mathbf{p} with integer coefficients. For the same exemplary model as above, the output file reads

```
quenchCoef = {
py (-2 h0) + px py (-4),
pz (8 + 4 h0^2) + py^2 (8 h1) + px (-4 h0 h1) + px pz (16 h0) + px^2
(-8 h1) + px^2 pz (8),
py (-48 h0 + -8 h0 h1^2 + -8 h0^3) + py pz (64 h0 h1) + px py (-64 +
-64 h1^2 + -48 h0^2) + px py pz (64 h1) + px^2 py (-48 h0)
};
```

Note that the imaginary unit is omitted in this file, so to get a quench coefficient (30) of the odd order one should multiply the entry of this file by i .

In addition, the program accepts several auxiliary flags to control its behavior and manage system resources:

- `-memory-limit ML`: Sets the memory limit for the program to ML megabytes. Because the number of Pauli strings grows exponentially, if the memory usage exceeds the RAM size, the OS automatically swaps the data to the disk. However, this swap procedure is hardware-dependent and can result in severe performance degradation or out-of-memory errors. Users are highly recommended to explicitly enforce a memory limit below the available RAM (with a reservation for other processes running simultaneously and consuming a part of RAM) by specifying this flag. The program will then safely handle the data chunking and its own optimized disk-writing.
- `-res-dir DIRECTORY`: Specifies a custom path where the directories with the results are to be saved (the default is `./tmp`).

Table 1: Maximal computed nesting order n_{\max} for the Ising model (19) (2D and 3D cases) or (35) (1D case) reported in various studies.

	2019 Parker <i>et al.</i> [19]	2021 Noh [54]	2024 De <i>et al.</i> [42]	2024 Uskov & Lychkovskiy [23]	2025 QCOMMUTE [30]
1D	30	38	35	45	48
2D	–	–	16	21	23
3D	–	–	–	–	17

- `-force`: Automatically deletes the contents of the target result directory before starting the computation. If the directory is not empty and this flag is omitted, the program will stop with an error message to prevent accidental mixing of old and new data.
- `-text-output`: Prints the final computed commutator to the standard output in a human-readable format. While useful for debugging at small n , it is not recommended for large nesting order due to a significant input/output overhead. Here is an example of such output for the 3rd commutator of the 1D Ising Model (35):

```
i*[-48,1,0;-8,1,2;-8,3,0]*Sy(1)
i*[32,0,1]*Sx(3)*Sy(1)*Sz(2)
i*[32,0,1]*Sx(1)*Sy(3)*Sz(2)
i*[-48,1,0]*Sx(1)*Sx(3)*Sy(2)
i*[32,1,1]*Sy(2)*Sz(1)
i*[-32;-32,0,2;-24,2,0]*Sx(2)*Sy(1)
i*[32,1,1]*Sy(1)*Sz(2)
i*[-32;-32,0,2;-24,2,0]*Sx(1)*Sy(2)
```

Finally, the package includes a standalone `validate [FILE1] [FILE2]` sub-command. This utility accepts two human-readable files containing sums of Pauli strings and explicitly reports whether the sums match, making it a valuable tool for debugging and cross-verifying results with other software.

3.4 Crosschecks

We have validated the results produced by our package by comparing them with results obtained for lower nesting orders using three independent software tools. First, for one-dimensional systems, we implemented a simplified version of our algorithm in WOLFRAM MATHEMATICA[®]. The second tool is a computer program (currently unsupported) written by Filipp Uskov in the FORM language. This program was used in Refs. [23, 47], where results for two-dimensional systems were reported. Finally, for three-dimensional systems, we compared our results with those obtained using the code by Igor Ermakov [31, 43]. In addition, we have cross-checked our results against exactly solvable cases – the one-dimensional transverse-field Ising model, as well as the classical Ising model in arbitrary dimension, given by eq. (19) with $h_z = 0$.

3.5 Performance

In order to highlight the growth of operator size and computational complexity with nesting order and demonstrate the efficiency of QCOMMUTE in addressing this growth, we perform computations for the Ising model on 1D, 2D, and 3D hypercubic lattices. The observable considered is the magnetization (20). In the 2D and 3D cases, the Hamiltonian is given by

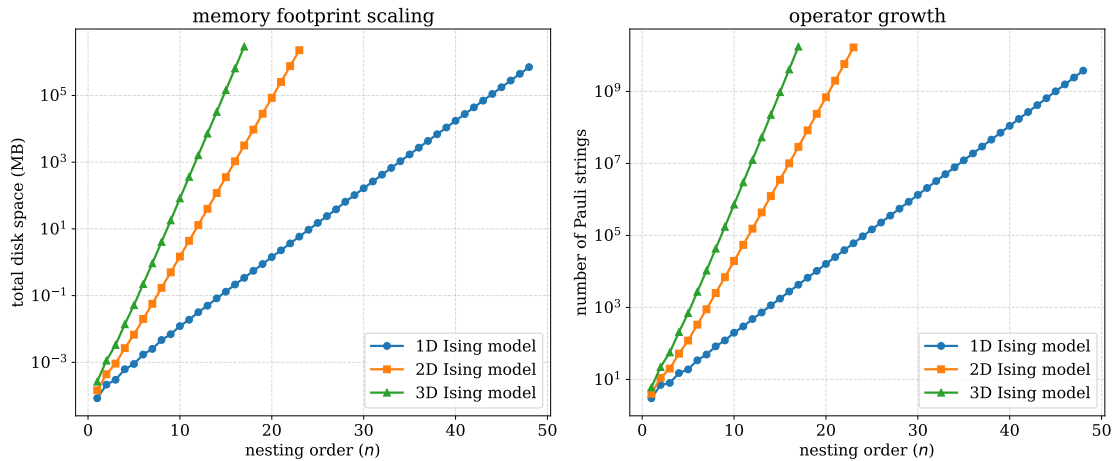


Figure 1: Scaling of the memory footprint (left) and the total number of unique Pauli strings (right) as a function of the nesting order n for the 2D and 3D transverse-field Ising model (19), and the 1D mixed-field Ising model (35). The algorithm avoids out-of-memory errors by dynamically caching operators on the disk.

eq. (19). In one dimension, the Hamiltonian (19) is exactly solvable; as a consequence, $\mathcal{L}^n A$ do not feature exponential growth and admit a relatively simple analytical form [44, 45, 48]. For this reason, in the 1D case we address the nonintegrable *mixed-field* Ising model with the Hamiltonian

$$H_{1D} = \sum_j \sigma_j^x \sigma_{j+1}^x + h_x \sum_j \sigma_j^x + h_z \sum_j \sigma_j^z. \quad (35)$$

As shown in Fig. 1, while the computational complexity grows exponentially at any dimensionality, the growth exponent is highly sensitive to the dimensionality. In the 1D case, this exponent is relatively low, allowing the program to comfortably reach $n_{\max} = 47$ at a 1 TB RAM server without swapping. At this nesting order, the expansion produces approximately 2.4×10^9 unique Pauli strings, occupying merely 428 GB of disk space.

Conversely, in the 2D and 3D cases the exponent is considerably larger, inducing a rapid exponential explosion of the number of Pauli strings and the memory usage. The true advantage of the disk-caching algorithm becomes evident already in the 2D case. Standard approaches relying solely on Random Access Memory (RAM) would face an inevitable out-of-memory (OOM) crash before reaching $n \simeq 20$ (at a 1 TB RAM server). By shifting the workload to NVMe (non-volatile memory express) storage, our software successfully handles over 1.7×10^{10} unique terms at $n = 23$ (consuming roughly 2,16 TB of disk space).

In Table 1, we list state-of-the-art maximal nesting orders computed for the transverse Ising model (19) on two- and three-dimensional hypercubic lattices and for the mixed-field one-dimensional Ising model (35), as reported in the literature, and compare them with the results obtained using QCOMMUTE [30]. We include only results free of boundary effects, i.e., those obtained either directly in the thermodynamic limit or for sufficiently large finite systems such that, for a given n_{\max} , the results coincide with the thermodynamic-limit values. While a fair comparison between different software packages would require benchmarking on identical hardware, the figures in Table 1 nevertheless indicate that QCOMMUTE performs favorably compared to other available tools.

Note that ref. [23], although sharing one author with the present work, reports results obtained using a different tool written in the FORM language. Among the listed implementations, only this code and QCOMMUTE support symbolic computations with Hamiltonian parameters

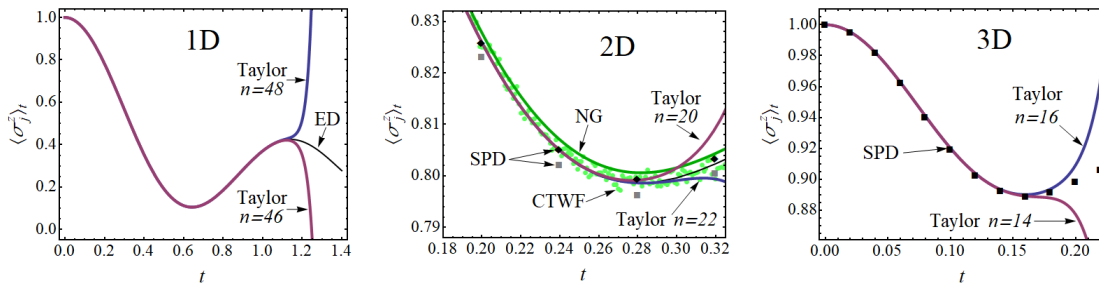


Figure 2: Quench dynamics of the quantum Ising model on one-, two-, and three-dimensional hypercubic lattices. The observable is the polarization per site in the z -direction, and the initial state is a product state fully polarized along z . The blue (magenta) line shows the Taylor expansion (8) truncated at the maximal available even order n_{\max}^{even} (at the order $(n_{\max}^{\text{even}} - 2)$), see text for details. **1D**: Results are shown for the mixed-field Ising model (35) with $h_x = h_z = 1$. The black line represents the exact diagonalization result, which is essentially indistinguishable from the thermodynamic-limit result on the time scale shown. **2D**: Results are shown for the transverse-field Ising model (19) at the critical field $h_z = 3.04438$. For comparison, we also show results obtained using other methods: black line – iPEPS [5], green line – NG [16], green points – CTWF [17], black diamonds – SPD with Trotter step $\delta t = 0.001$ [28], and gray squares – SPD with $\delta t = 0.004$ [28]. **3D**: Results are shown for the transverse-field Ising model (19) at the critical field $h_z = 5.15813$. The black line shows the SPD result [28].

kept analytic, whereas other tools perform computations for specific numerical values of these parameters. We also note that Ref. [42] reports two-dimensional results for a slightly more complex mixed-field Ising model.

4 An application: short-time dynamics of quantum Ising model

Here we apply QCOMMUTE to study short-time dynamics of the one-dimensional mixed-field Ising model (35) and the two- and three-dimensional transverse-field Ising model (19). As the observable, we consider the total magnetization (20).

We first consider a quantum quench from the product state (29) polarized along the z -direction, $\mathbf{p} = (0, 0, 1)$, with the results shown in Fig. 2. We compute the quench coefficients (9) and use them to approximate the post-quench dynamics of the magnetization via the truncated Taylor expansion (8). For this particular initial state, the odd quench coefficients (9) vanish identically. This follows from T -invariance and can be verified directly by taking the complex conjugate of Eq. (9). Accordingly, we present results for truncation orders n_{\max}^{even} and $(n_{\max}^{\text{even}} - 2)$. The coincidence of the two curves determines the time interval over which the approximation is reliable.

We compare our results with other available methods. In one dimension, we benchmark against exact diagonalization (ED) of a spin chain with $N = 12$ sites and periodic boundary conditions. We have verified that this system size is sufficient for the results to be effectively indistinguishable from those in the thermodynamic limit on the time scales considered.

In two dimensions, we compare our results with those obtained using the infinite projected entangled pair state (iPEPS) [5], the sparse Pauli dynamics (SPD) [28], the time-dependent neural Galerkin (NG) [16] methods, and the time-dependent variational principle with convolutional transformer wave functions (CTWF) [17]. As noted recently in Ref. [9], there is a

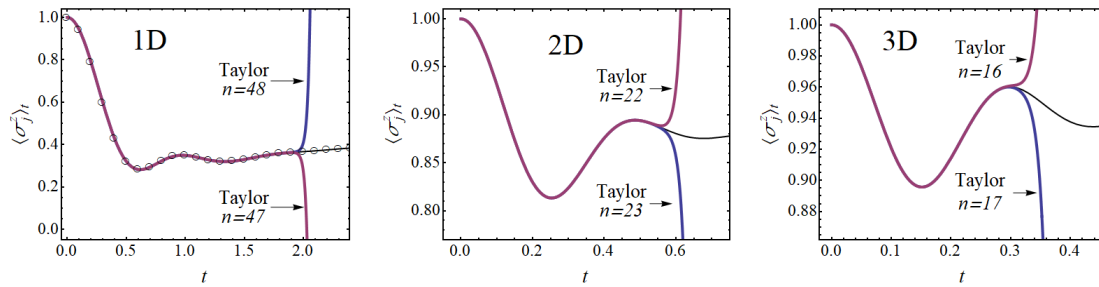


Figure 3: Autocorrelation function for the quantum Ising model on one-, two-, and three-dimensional hypercubic lattices. The observable and the Hamiltonians are the same as in Fig. 2. The blue (magenta) line shows the Taylor expansion (10) truncated at the maximal available order n_{\max} (at the order $(n_{\max} - 1)$). The black line shows the results of the recursion method [23, 30]. Additionally, in the 1D case the exact diagonalization result is shown by open circles.

small discrepancy between the iPEPS and SPD results on the one hand and the NG results on the other. Our results agree with the iPEPS and most accurate (i.e. those obtained with the smallest available Trotter time step) SPD data, thus providing an independent high-precision benchmark. In contrast, the CTWF results exhibit noise at a level comparable to this discrepancy and therefore do not resolve it.

In three dimensions, we compare our results with those obtained using SPD, which, to the best of our knowledge, provides the only independent results currently available in three dimensions. We find excellent agreement.

Next, we consider the autocorrelation function (10). The upper and lower bounds (12) obtained from the Taylor expansion are shown in Fig. 3. In one dimension, we again benchmark against essentially exact results from exact diagonalization. In two and three dimensions, where independent benchmarks are scarce, we compare instead with results obtained using the recursion method [23, 30], which relies on the same moments μ_{2n} that enter Eqs. (10), (12). One can see from Fig. 3 that the recursion-method results lie within the Taylor bounds (12), as they should. Observe that, up to a certain time, the two-sided bound (12) is extremely tight, effectively yielding the exact autocorrelation function.

5 Summary and outlook

To summarize, the QCOMMUTE package [1] is a highly effective tool for computing nested commutators between translation-invariant operators in spin-1/2 systems on one-, two-, and three-dimensional hypercubic lattices. It has the following distinctive features:

- it operates directly in the thermodynamic limit (infinite lattice, no boundary effects);
- it treats Hamiltonian parameters symbolically, so that a single run produces results across the entire parameter space;
- it employs extensive and highly optimized parallelization.

This combination of features makes QCOMMUTE unique among existing tools for computing nested commutators, each of which typically supports only a subset of these capabilities. The first feature is particularly distinctive: PAULISTRINGS.JL [34, 35], PAULIPROPAGATION.JL [36], and the SPD package [27, 28] all operate on finite lattices. While, for a given nesting order, the

infinite-lattice result can be reproduced exactly using a finite lattice whose linear size is proportional to this order (as explained in Section 2.3), this approach incurs a substantial memory overhead, which is critical since memory is the primary bottleneck in these computations.

As for the symbolic treatment of Hamiltonian parameters, it is implemented in PAULIPROPAGATION.JL, but not in PAULISTRINGS.JL or the spd package. Remarkably, retaining parameters in symbolic form incurs only moderate overhead in both memory and runtime compared to a purely numerical computation, owing to the inherently computer-algebraic nature of the algorithm. This feature is particularly advantageous when results are required for multiple points in parameter space: a single symbolic computation can be reused to obtain results for arbitrary parameter values [23, 30, 31, 36, 55]. Another, less obvious advantage of representing results as polynomials in the parameters with integer coefficients, rather than as floating-point numbers, arises in the context of the recursion method. There the symbolic representation helps to avoid numerical instabilities [23, 30, 47] that otherwise plague the method [56].

While QCOMMUTE has been developed with an emphasis on computational efficiency, flexibility is not currently its main strength. Enhancing flexibility is therefore a natural direction for future development. In particular, it would be desirable to extend the functionality of the code to support lattices beyond the hypercubic ones. Furthermore, it would be advantageous to implement the computation of quench coefficients for arbitrary initial states, rather than restricting to product states (29). Beyond these largely technical improvements, a more substantial extension would be the direct implementation of the Pauli propagation algorithm [27, 28] within the package, fully leveraging its advanced parallelization and memory-management capabilities.

Acknowledgements

We are grateful to Igor Ermakov for useful discussions and, in particular, for providing validation data for the three-dimensional Ising model.

Author contributions All three authors contributed to the development of the algorithm. OL initiated the project, developed a WOLFRAM MATHEMATICA[®] code to validate the results for one-dimensional systems, and applied the results to physical problems. ISh implemented the algorithm in C++. VH and ISh improved the performance of the code, with particular emphasis on parallelization and memory management. The manuscript was written by OL and ISh.

Funding information This work was supported by the Russian Science Foundation under grant № 24-22-00331 <https://rscf.ru/en/project/24-22-00331/>

References

- [1] QCOMMUTE, <https://github.com/QCommute> (2026).
- [2] U. Schollwöck, *The density-matrix renormalization group in the age of matrix product states*, *Annals of Physics* **326**(1), 96 (2011), doi:<https://doi.org/10.1016/j.aop.2010.09.012>, January 2011 Special Issue.
- [3] M. Fishman, S. R. White and E. M. Stoudenmire, *The ITensor Software Library for Tensor Network Calculations*, *SciPost Phys. Codebases* p. 4 (2022), doi:[10.21468/SciPostPhysCodeb.4](https://doi.org/10.21468/SciPostPhysCodeb.4).

- [4] M. Fishman, S. R. White and E. M. Stoudenmire, *Codebase release 0.3 for ITensor*, SciPost Phys. Codebases pp. 4–r0.3 (2022), doi:[10.21468/SciPostPhysCodeb.4-r0.3](https://doi.org/10.21468/SciPostPhysCodeb.4-r0.3).
- [5] J. Dziarmaga, *Time evolution of an infinite projected entangled pair state: A gradient tensor update in the tangent space*, Phys. Rev. B **106**, 014304 (2022), doi:[10.1103/PhysRevB.106.014304](https://doi.org/10.1103/PhysRevB.106.014304).
- [6] T. Hashizume, I. P. McCulloch and J. C. Halimeh, *Dynamical phase transitions in the two-dimensional transverse-field ising model*, Phys. Rev. Res. **4**, 013250 (2022), doi:[10.1103/PhysRevResearch.4.013250](https://doi.org/10.1103/PhysRevResearch.4.013250).
- [7] S. De Nicola, A. A. Michailidis and M. Serbyn, *Entanglement and precession in two-dimensional dynamical quantum phase transitions*, Phys. Rev. B **105**, 165149 (2022), doi:[10.1103/PhysRevB.105.165149](https://doi.org/10.1103/PhysRevB.105.165149).
- [8] R. Kaneko and I. Danshita, *Dynamics of correlation spreading in low-dimensional transverse-field ising models*, Phys. Rev. A **108**, 023301 (2023), doi:[10.1103/PhysRevA.108.023301](https://doi.org/10.1103/PhysRevA.108.023301).
- [9] G. Park, J. Gray and G. K.-L. Chan, *Simulating quantum dynamics in two-dimensional lattices with tensor network influence functional belief propagation*, Phys. Rev. B **112**, 174310 (2025), doi:[10.1103/7jzt-xhn6](https://doi.org/10.1103/7jzt-xhn6).
- [10] L. Pavešić, D. Jaschke and S. Montangero, *Constrained dynamics and confinement in the two-dimensional quantum ising model*, Phys. Rev. B **111**, L140305 (2025), doi:[10.1103/PhysRevB.111.L140305](https://doi.org/10.1103/PhysRevB.111.L140305).
- [11] S. Mandrà, N. Astrakhantsev, S. Isakov, B. Villalonga, B. Ware, T. Westerhout and K. Kechedzhi, *A heuristic for matrix product state simulation of out-of-equilibrium dynamics of two-dimensional transverse-field ising models*, arXiv preprint arXiv:2511.23438 (2025).
- [12] J. Vovrosh, S. Julià-Farré, W. Krinitsin, M. Kaicher, F. Hayes, E. Gottlob, A. Kshetri-mayum, K. Bidzhiev, S. B. Jäger, M. Schmitt *et al.*, *Simulating dynamics of the two-dimensional transverse-field ising model: a comparative study of large-scale classical numerics*, arXiv:2511.19340 (2025).
- [13] M. Schmitt and M. Heyl, *Quantum many-body dynamics in two dimensions with artificial neural networks*, Phys. Rev. Lett. **125**, 100503 (2020), doi:[10.1103/PhysRevLett.125.100503](https://doi.org/10.1103/PhysRevLett.125.100503).
- [14] F. Vicentini, D. Hofmann, A. Szabó, D. Wu, C. Roth, C. Giuliani, G. Pescia, J. Nys, V. Vargas-Calderón, N. Astrakhantsev and G. Carleo, *NetKet 3: Machine Learning Toolbox for Many-Body Quantum Systems*, SciPost Phys. Codebases p. 7 (2022), doi:[10.21468/SciPostPhysCodeb.7](https://doi.org/10.21468/SciPostPhysCodeb.7).
- [15] F. Vicentini, D. Hofmann, A. Szabó, D. Wu, C. Roth, C. Giuliani, G. Pescia, J. Nys, V. Vargas-Calderón, N. Astrakhantsev and G. Carleo, *Codebase release 3.4 for NetKet*, SciPost Phys. Codebases pp. 7–r3.4 (2022), doi:[10.21468/SciPostPhysCodeb.7-r3.4](https://doi.org/10.21468/SciPostPhysCodeb.7-r3.4).
- [16] A. Sinibaldi, D. Hendry, F. Vicentini and G. Carleo, *Time-dependent neural galerkin method for quantum dynamics*, arXiv:2412.11778 (2024).
- [17] A. Chen, V. D. Naik and M. Heyl, *Convolutional transformer wave functions*, arXiv:2503.10462 (2025).

- [18] G. A. Starkov and B. V. Fine, *Hybrid quantum-classical method for simulating high-temperature dynamics of nuclear spins in solids*, Phys. Rev. B **98**, 214421 (2018), doi:[10.1103/PhysRevB.98.214421](https://doi.org/10.1103/PhysRevB.98.214421).
- [19] D. E. Parker, X. Cao, A. Avdoshkin, T. Scaffidi and E. Altman, *A universal operator growth hypothesis*, Phys. Rev. X **9**, 041017 (2019), doi:[10.1103/PhysRevX.9.041017](https://doi.org/10.1103/PhysRevX.9.041017).
- [20] V. Khemani, A. Vishwanath and D. A. Huse, *Operator spreading and the emergence of dissipative hydrodynamics under unitary evolution with conservation laws*, Phys. Rev. X **8**, 031057 (2018), doi:[10.1103/PhysRevX.8.031057](https://doi.org/10.1103/PhysRevX.8.031057).
- [21] T. Rakovszky, C. W. von Keyserlingk and F. Pollmann, *Dissipation-assisted operator evolution method for capturing hydrodynamic transport*, Phys. Rev. B **105**, 075131 (2022), doi:[10.1103/PhysRevB.105.075131](https://doi.org/10.1103/PhysRevB.105.075131).
- [22] C. D. White, *Effective dissipation rate in a liouvillian-graph picture of high-temperature quantum hydrodynamics*, Phys. Rev. B **107**, 094311 (2023), doi:[10.1103/PhysRevB.107.094311](https://doi.org/10.1103/PhysRevB.107.094311).
- [23] F. Uskov and O. Lychkovskiy, *Quantum dynamics in one and two dimensions via the recursion method*, Phys. Rev. B **109**, L140301 (2024), doi:[10.1103/PhysRevB.109.L140301](https://doi.org/10.1103/PhysRevB.109.L140301).
- [24] I. Ermakov, O. Lychkovskiy and T. Byrnes, *Unified framework for efficiently computable quantum circuits*, arXiv:2401.08187 (2024).
- [25] N. Loizeau, B. Buča and D. Sels, *Opening krylov space to access all-time dynamics via dynamical symmetries*, Phys. Rev. Lett. **135**, 200401 (2025), doi:[10.1103/PhysRevLett.135.200401](https://doi.org/10.1103/PhysRevLett.135.200401).
- [26] A. Angrisani, A. A. Mele, M. S. Rudolph, M. Cerezo and Z. Holmes, *Simulating quantum circuits with arbitrary local noise using pauli propagation*, arXiv preprint arXiv:2501.13101 (2025).
- [27] T. Begušić, J. Gray and G. K.-L. Chan, *Fast and converged classical simulations of evidence for the utility of quantum computing before fault tolerance*, Science Advances **10**(3), eadk4321 (2024), doi:[10.1126/sciadv.adk4321](https://doi.org/10.1126/sciadv.adk4321).
- [28] T. Begušić and G. K.-L. Chan, *Real-time operator evolution in two and three dimensions via sparse pauli dynamics*, PRX Quantum **6**, 020302 (2025), doi:[10.1103/PRXQuantum.6.020302](https://doi.org/10.1103/PRXQuantum.6.020302).
- [29] A. Teretenkov, F. Uskov and O. Lychkovskiy, *Pseudomode expansion of many-body correlation functions*, Phys. Rev. B **111**, 174308 (2025), doi:[10.1103/PhysRevB.111.174308](https://doi.org/10.1103/PhysRevB.111.174308).
- [30] I. Shirokov, V. Khrushchev, F. Uskov, I. Dudinets, I. Ermakov and O. Lychkovskiy, *Quench dynamics via recursion method*, arXiv:2503.24362 (2025).
- [31] I. Ermakov and O. Lychkovskiy, *Symbolic recursion method for strongly correlated fermions in two and three dimensions*, arXiv preprint arXiv:2512.23678 (2025).
- [32] H. Mori, *A continued-fraction representation of the time-correlation functions*, Progress of Theoretical Physics **34**(3), 399 (1965), doi:[10.1143/PTP.34.399](https://doi.org/10.1143/PTP.34.399).
- [33] V. Viswanath and G. Müller, *The Recursion Method: Application to Many-Body Dynamics*, vol. 23, Springer Science & Business Media (2008).

- [34] N. Loizeau, J. C. Peacock and D. Sels, *Quantum many-body simulations with PauliStrings.jl*, SciPost Phys. Codebases p. 54 (2025), doi:[10.21468/SciPostPhysCodeb.54](https://doi.org/10.21468/SciPostPhysCodeb.54).
- [35] N. Loizeau, J. C. Peacock and D. Sels, *Codebase release 1.5 for PauliStrings.jl*, SciPost Phys. Codebases pp. 54–r1.5 (2025), doi:[10.21468/SciPostPhysCodeb.54-r1.5](https://doi.org/10.21468/SciPostPhysCodeb.54-r1.5).
- [36] M. S. Rudolph, T. Jones, Y. Teng, A. Angrisani and Z. Holmes, *Pauli propagation: A computational framework for simulating quantum systems*, arXiv preprint arXiv:2505.21606 (2025).
- [37] T. Begušić, *Sparse Pauli Dynamics (SPD) Python implementation*, <https://github.com/tbegusic/spd/tree/main/spd>, Accessed: 2026-03-25.
- [38] J. Roldan, B. M. McCoy and J. H. Perk, *Dynamic spin correlation functions of the xyz chain at infinite temperature: A study based on moments*, Physica A: Statistical Mechanics and its Applications **136**(2), 255 (1986), doi:[https://doi.org/10.1016/0378-4371\(86\)90254-2](https://doi.org/10.1016/0378-4371(86)90254-2).
- [39] J. Florencio, S. Sen and Z. Cai, *Quantum spin dynamics of the transverse ising model in two dimensions*, Journal of Low Temperature Physics **89**, 561 (1992), doi:[10.1007/BF00694087](https://doi.org/10.1007/BF00694087).
- [40] N. H. Lindner and A. Auerbach, *Conductivity of hard core bosons: A paradigm of a bad metal*, Phys. Rev. B **81**, 054512 (2010), doi:[10.1103/PhysRevB.81.054512](https://doi.org/10.1103/PhysRevB.81.054512).
- [41] E. W. Huang, R. Sheppard, B. Moritz and T. P. Devereaux, *Strange metallicity in the doped hubbard model*, Science **366**(6468), 987 (2019), doi:[10.1126/science.aau7063](https://doi.org/10.1126/science.aau7063).
- [42] A. De, U. Borla, X. Cao and S. Gazit, *Stochastic sampling of operator growth dynamics*, Phys. Rev. B **110**, 155135 (2024), doi:[10.1103/PhysRevB.110.155135](https://doi.org/10.1103/PhysRevB.110.155135).
- [43] I. Ermakov, *Operator growth in many-body systems of higher spins*, arXiv:2504.07833 (2025).
- [44] T. Prosen, *Exact time-correlation functions of quantum ising chain in a kicking transversal magnetic field: Spectral analysis of the adjoint propagator in Heisenberg picture*, Progress of Theoretical Physics Supplement **139**, 191 (2000), doi:[10.1143/PTPS.139.191](https://doi.org/10.1143/PTPS.139.191).
- [45] O. Lychkovskiy, *Closed hierarchy of Heisenberg equations in integrable models with Onsager algebra*, SciPost Phys. **10**, 124 (2021), doi:[10.21468/SciPostPhys.10.6.124](https://doi.org/10.21468/SciPostPhys.10.6.124).
- [46] O. Gamayun and O. Lychkovskiy, *Out-of-equilibrium dynamics of the Kitaev model on the Bethe lattice via coupled Heisenberg equations*, SciPost Phys. **12**, 175 (2022), doi:[10.21468/SciPostPhys.12.5.175](https://doi.org/10.21468/SciPostPhys.12.5.175).
- [47] A. Teretenkov and O. Lychkovskiy, *Exact dynamics of quantum dissipative XX models: Wannier-Stark localization in the fragmented operator space*, Physical Review B **109**(14), L140302 (2024), doi:[10.1103/PhysRevB.109.L140302](https://doi.org/10.1103/PhysRevB.109.L140302).
- [48] I. Ermakov, T. Byrnes and O. Lychkovskiy, *Polynomially restricted operator growth in dynamically integrable models*, Phys. Rev. B **111**, 094314 (2025), doi:[10.1103/PhysRevB.111.094314](https://doi.org/10.1103/PhysRevB.111.094314).
- [49] P. Penc and F. H. L. Essler, *Linear response and exact hydrodynamic projections in Lindblad equations with decoupled Bogoliubov hierarchies*, SciPost Phys. **20**, 058 (2026), doi:[10.21468/SciPostPhys.20.2.058](https://doi.org/10.21468/SciPostPhys.20.2.058).

- [50] O. Gamayun, M. A. Mir, O. Lychkovskiy and Z. Ristivojevic, *Exactly solvable models for universal operator growth*, J. High Energ. Phys. **2025**, 256 (2025), doi:[10.1007/JHEP07\(2025\)256](https://doi.org/10.1007/JHEP07(2025)256).
- [51] N. Angelinos, D. Chakraborty and A. Dymarsky, *Temperature dependence in krylov space*, arXiv preprint arXiv:2508.19233 (2025).
- [52] H. Araki, *Gibbs states of a one dimensional quantum lattice*, Communications in Mathematical Physics **14**, 120 (1969).
- [53] V. Khrushchev, O. Lychkovskiy and I. Shirokov, *COMMUTE source code repository*, https://gitlab.com/viacheslav_hrushev/commutators (2025).
- [54] J. D. Noh, *Operator growth in the transverse-field ising spin chain with integrability-breaking longitudinal field*, Phys. Rev. E **104**, 034112 (2021), doi:[10.1103/PhysRevE.104.034112](https://doi.org/10.1103/PhysRevE.104.034112).
- [55] M. S. Rudolph, E. Fontana, Z. Holmes and L. Cincio, *Classical surrogate simulation of quantum systems with lowesa*, arXiv preprint arXiv:2308.09109 (2023).
- [56] J. Ecksele, M. Pieper and J. Schnack, *Escaping the krylov space during the finite-precision lanczos algorithm*, Phys. Rev. E **112**, 025306 (2025), doi:[10.1103/k94p-vls8](https://doi.org/10.1103/k94p-vls8).